Inter-Turn Short-Circuit Fault Detection Approach for Permanent Magnet Synchronous Machines Through Stray Magnetic Field Sensing

Xuyang Liu, *Student Member, IEEE*, Wenchao Miao, Qi Xu, Libing Cao, *Student Member, IEEE*, Chunhua Liu, *Senior Member, IEEE*, and Philip W. T. Pong, *Senior Member, IEEE*

***Abstract*— Fast online detection of inter-turn short-circuit faults for permanent magnet synchronous machines (PMSMs) is a challenging task. Previous attempts based on phase currents or back EMF monitoring lack the capability to accurately locate the inter-turn short-circuit faults in stator windings. This paper proposed a new approach to online inter-turn short-circuit fault detection for PMSMs by means of sensing the external stray magnetic field outside the motor stator yoke. The stray magnetic field provides the information about the phase currents as well as the status of stator windings and thus, the location of inter-turn short-circuit fault can be detected accordingly. In this paper, the inter-turn short-circuit model and the stray magnetic flux model for PMSMs were theoretically analyzed. Both FEM simulations and experiments have been presented to validate the effectiveness of the proposed approach. A sensor array composed of 24 sensitive tunneling magnetoresistive (TMR) sensor units was employed to measure the stray magnetic field distribution outside the PMSM stator yoke. The experimental results show that both the location and severity of the inter-turn short-circuit fault in PMSMs were effectively detected using the proposed approach.**

***Index Terms*— Inter-turn short-circuit faults, online fault detection, permanent magnet synchronous machine (PMSM), stray magnetic field, tunneling magnetoresistive (TMR) sensors.**

I. Introduction

DUE to the advantages such as high efficiency, high power density, and high power-to-volume ratio, permanent magnet synchronous machines (PMSMs) have attracted considerable interest in many industrial applications [1]–[3]. Unexpected faults or failures of PMSMs could lead to costly repair or replacement, or even a catastrophic system failure in several mission-critical applications. Therefore, the reliable and valid health monitoring and early fault-diagnostic are highly desired to ensure the high performance of PMSMs over long periods of time. From a number of literature [4]–[8], it is deduced that stator winding short-circuit faults due to coil insulation degradation resulting from thermal stress comprise a large proportion of electrical faults. Studies show that 80% of electrical failures result from the inter-turn short-circuit fault [9]. More seriously, an inter-turn short-circuit fault inside stator windings can easily expand into nearby coils, which gradually aggravate the severity of short-circuit faults [10]. However, by far the online inter-turn winding short-circuit fault diagnosis for PMSMs is still a challenging task.

By reviewing the past work, it is apparent that the existing frequently-used approach to detect the short-circuit faults is based on motor current signature analysis (MCSA) [8], [11]–[16]. The frequency analysis of stator currents by means of short-time FFT [11] or wavelet transform [15] can be easily implemented for fault detection. However, fault signatures in the stator current spectrum highly depend on the winding configuration, winding type, fault location, load conditions, etc. As an inter-turn short-circuit fault results into the imbalance in the three-phase impedance, and thus an unbalanced operating condition, negative sequence components [17], [18], impedance changes [19], and control voltages [20] can be measured to detect the inter-turn short-circuit faults. However, these fault detection methods highly rely on the predefined fault threshold level which requires vast pre-calibration data. Moreover, all the above-mentioned approaches cannot locate the inter-turn short-circuit faults in stator windings.

Several studies have addressed the leakage flux usage for condition monitoring in asynchronous machines [21]–[24]. The stray flux of a PMSM that radiates out of the machine can provide the stator information inside the motor. It is claimed that stray magnetic flux is more efficient than stator current for detecting faults, particularly in the no-load operating condition. More importantly, the stray magnetic signature can provide information concerning the location of the fault [25]. However, the majority of stray field sensing for motors in the previous work is based on the external search coil [21], [24]–[26], use of which has major drawbacks including bulky size, complex installation, etc. For example, one way to implement search coils is to make them wound around

Manuscript received May 1, 2019; accepted May 14, 2019. Date of publication May 20, 2019; date of current version August 15, 2019. This work was supported in part by the Seed Funding Program for Basic Research, in part by the Seed Funding Program for Applied Research, in part by the Small Project Funding Program from The University of Hong Kong, in part by the ITF Tier 3 under Grant ITS/203/14, Grant ITS/104/13, Grant ITS/214/14, in part by RGC-GRF under Grant HKU 17210014 and Grant HKU 17204617, and in part by the University Grants Committee of Hong Kong under Contract AoE/P-04/08. The associate editor coordinating the review of this paper and approving it for publication was Prof. Pai-Yen Chen. *(Corresponding author: Philip W. T. Pong.)*

X. Liu, W. Miao, Q. Xu, L. Cao, and P. W. T. Pong are with the Department of Electrical and Electronic Engineering, The University of Hong Kong, Hong Kong (e-mail: ppong@eee.hku.hk).

C. Liu is with the School of Energy and Environment, City University of Hong Kong, Hong Kong (e-mail: chualiu@cityu.edu.hk).

Digital Object Identifier 10.1109/JSEN.2019.2918018

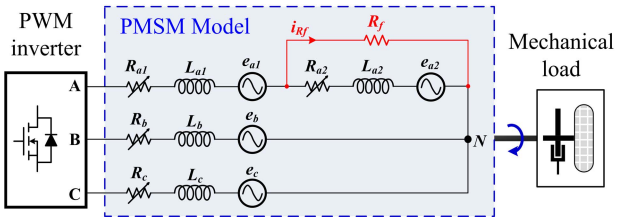

Fig. 1. PMSM model with inter-turn short-circuit fault in phase a.

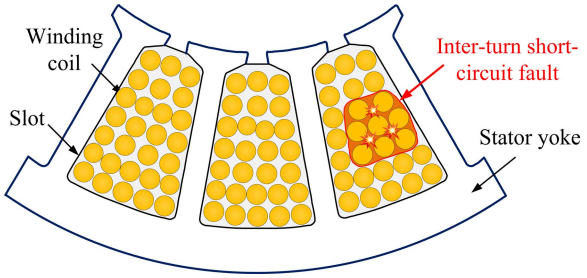

Fig. 2. Cross-section of the inter-turn short-circuit fault in stator winding.

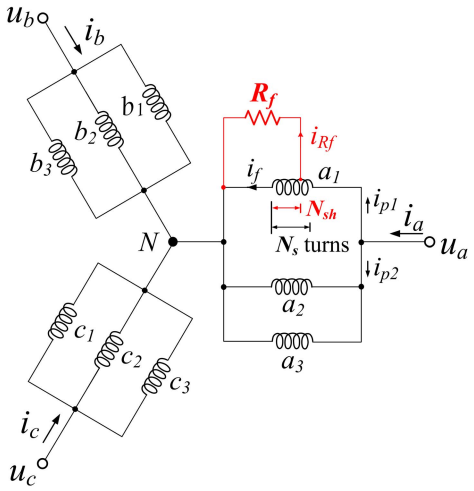

Fig. 3. Parallel-connected winding with inter-turn short-circuit fault in phase a.

the stator teeth of electric machines during the manufacturing process [25].

This paper proposes an approach to inter-turn short-circuit faults detection through stray magnetic field sensing by means of compact-in-size tunneling magnetoresistive (TMR) sensors. Comparing to the search coils, TMR sensors are the more promising candidates for stray magnetic field sensing in PMSMs [27]–[30]. The compactness of TMR sensors allows easier installation and replacement outside the motor stator yoke when the PMSM is still operating. TMR sensors provide much higher sensitivity with wide frequency bandwidth (i.e., up to a few MHz). Moreover, TMR sensors also provide direction-sensitive outputs so that both the radial and tangential components can be obtained using one sensor unit. By analyzing the stray magnetic fields, the operating condition of the stator windings can be estimated effectively. The location of the inter-turn short-circuit fault can be accurately detected by the implementation of 24 TMR sensor units. This new approach to online inter-turn short-circuit fault diagnostic through stray magnetic field sensing can achieve the intelligent and reliable health monitoring of stator winding for PMSMs.

This paper is organized as follows. The PMSM model with the inter-turn short-circuit fault and the operating principle of short-circuit detection are presented in Section II and Section III, respectively. The simulation analysis using finite element analysis was performed in Section IV to predict the stray magnetic fields of the faulty motor. Section V demonstrates the experimental validation of the proposed approach using a PMSM testbed under various operating conditions. Section VI finally addresses the conclusion of this work.

II. PMSM Model With Inter-Turn Short-Circuit

A PMSM model with the inter-turn short-circuit fault in stator winding concerning the dynamic and steady-state equations is presented in this section. Fig. 1 depicts the general PMSM model with the inter-turn short-circuit fault in phase a. Phase a is divided into the healthy part (a_1) and the faulty part (a_2) due to the inter-turn short-circuit fault. As shown in Fig. 2, the winding-coil insulation gradually deteriorates due to the high voltage and thermal pressure and then an inter-turn short-circuit fault inside the stator slot occurs. The shorted coils do not provide a zero resistance path. Instead, the short-circuit fault spot is generally modeled by a fault resistor R_f with the short-circuit fault current i_f [31].

More specifically, an inter-turn short-circuit fault model for PMSMs with parallel-connected winding configuration is illustrated in Fig. 3. Here, a_1, a_2, a_3, b_1, b_2, b_3, c_1, c_2, and c_3 are the stator windings of each phase; u_a, u_b, and u_c denote the voltages of three-phase windings; i_a, i_b, and i_c denote the phase currents; i_{p1}, i_{p2}, and i_{Rf} denote the current of the remanant healthy winding (a_1), other windings (a_2 and a_3) and the fault resistor (R_f), respectively. Without the short-circuit fault, i_{p1}, i_{p2}, and i_{Rf} are $i_a/3$, $2i_a/3$, and zero, respectively. When a short-circuit fault occurs, the impedance in the winding a_1 decreases, then i_{p1} and i_{p2} change in both the magnitude and phase, and a non-zero i_{Rf} is induced consequently.

For an inverter-fed PMSM, the phase currents can be simply expressed as

$$i_a = -I_q \sin\theta + I_d \cos\theta \tag{1}$$

$$i_b = -I_q \sin(\theta - 2\pi/3) + I_d \cos(\theta - 2\pi/3) \tag{2}$$

$$i_c = -I_q \sin(\theta + 2\pi/3) + I_d \cos(\theta + 2\pi/3) \tag{3}$$

where I_d and I_q denote the d-q axis currents in a synchronous rotating reference frame, respectively.

According to the previous literatures [10], [32], the magnetic flux linkage of the a-phase winding with the inter-turn short–circuit fault is expressed as

$$\begin{bmatrix} \lambda_{a1h} \\ \lambda_{a2} = \lambda_{a3} \\ \lambda_{a1f} \end{bmatrix} = \boldsymbol{L}_{\mathbf{sm}} \begin{bmatrix} i_{p1} \\ i_{p2} \\ i_f \end{bmatrix} + \begin{bmatrix} -xL_m/2 \\ -L_m/2 \\ (x-1)L_m/2 \end{bmatrix} \times L_m(i_b + i_c) \tag{4}$$

where λ_{a2}, λ_{a2}, λ_{a1h}, and λ_{a1f} denote the flux linkage of winding a_2, winding a_3, the healthy and faulty parts of winding a_1, respectively, $\boldsymbol{L}_{\mathbf{sm}}$ is a coefficient matrix of winding

coupling factors, x denotes the healthy turn ratio of winding a_1 ($x = 1 - N_{sh}/N_s$), and L_m denotes the phase self-inductance.

Using the Eq. (4), the overall voltage dynamic equation of a parallel-connected PMSM with the inter-turn short-circuit fault is obtained as

$$\begin{bmatrix} u_a \\ u_a \\ u_b \\ u_c \\ 0 \end{bmatrix} = \boldsymbol{R}_p \begin{bmatrix} i_{p1} \\ i_{p2} \\ i_b \\ i_c \\ i_f \end{bmatrix} + \boldsymbol{L}_p \frac{d}{dt} \begin{bmatrix} i_{p1} \\ i_{p2} \\ i_b \\ i_c \\ i_f \end{bmatrix} + \omega k_E \begin{bmatrix} -x \sin\theta \\ -\sin\theta \\ -\sin(\theta - 2\pi/3) \\ -\sin(\theta + 2\pi/3) \\ (x-1)\sin\theta \end{bmatrix} \quad (5)$$

where $\boldsymbol{R}_P$ and $\boldsymbol{L}_p$ denote the coefficient matrixes of winding resistance and winding inductance coefficients (including self-inductances and mutual inductances among windings), respectively; ω and k_E denote the angular velocity and the back EMF constant, respectively.

Moreover, the steady-state equations for a PMSM with parallel-connected winding are also developed using the Laplace transform, with i_{p1} and i_f expressed as

$$i_{p1} = \alpha_1 \sin\theta + \alpha_2 \cos\theta \quad (6)$$

$$i_f = \beta_1 \sin\theta + \beta_2 \cos\theta \quad (7)$$

where α_1, α_2, β_1, and β_2 denote the coefficients of the sine and cosine function.

Substituting Eq. (6) and Eq. (7) into Eq. (5), the phase voltage equation can be given as

$$\begin{bmatrix} u_a \\ u_b \\ u_c \end{bmatrix} = \boldsymbol{R}_{p'} \begin{bmatrix} i_{p2} \\ i_b \\ i_c \end{bmatrix} + \omega k_E \begin{bmatrix} -\sin\theta \\ -\sin(\theta - 2\pi/3) \\ (x-1)\sin\theta \end{bmatrix} + \boldsymbol{L}_{p'} \frac{d}{dt} \begin{bmatrix} i_{p1} \\ i_{p2} \\ i_b \\ i_c \\ i_f \end{bmatrix} \quad (8)$$

Here, $\boldsymbol{R}_{P'}$ and $\boldsymbol{L}_{p'}$ are the submatrix of $\boldsymbol{R}_P$ and $\boldsymbol{L}_p$, respectively.

By multiplying the rotor flux linkage terms with the winding current, the torque equation can be given by

$$T = \frac{3}{2}\frac{P}{2} I_q k_E - \frac{P}{2}(1-x) k_E \sin\theta (i_f - i_{p1}) \quad (9)$$

From the above equations, the inter-turn short-circuit in a PMSM can be theoretically analyzed using the dynamic model and then the short-circuit fault can be detected accordingly. However, the location of the short-circuit fault cannot be detected by the phase currents and phase voltage values. A new approach to inter-turn short-circuit fault detection and localization through stray magnetic field sensing is proposed in this work and will be introduced in the following Section.

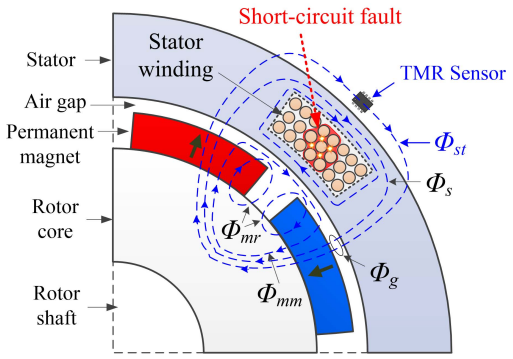

Fig. 4. An 8-pole SPMSM topology and the possible flux paths.

III. Principle of Short-Circuit Detection Through Stray Magnetic Field Sensing

In this Section, the magnetic equivalent circuit (MEC) method is employed to analyze the behavior of the stray magnetic field and its relationship to the inter-turn short-circuit fault in a surface-mounted permanent magnet synchronous motor (SPMSM). Fig. 4 depicts the cross-section of the simplified SPMSM topology and the possible flux paths. The stray leakage flux (Φ_{st}) originates from the stator current and radiates outside the stator yoke, thus it can provide the information about the stator currents as well as winding healthy conditions. When a short-circuit fault occurs inside the stator winding as shown in Fig. 4, the stray leakage flux behind the stator slot suffers from the changes in magnitude, which can be detected by using a sensitive TMR sensor.

More explicitly, the MEC model for the PMSM can be illustrated as Fig. 4. Here, F_s denotes the MMF source due to the stator windings in one slot, Φ_m denotes the flux source of the permanent magnet, R_{st}, R_r, R_g, R_s, R_t, R_l and represent the reluctance corresponding to stray leakage, rotor core, air-gap, stator core, stator teeth, magnet-to-magnet leakage and magnet-to-rotor leakage, respectively. The expressions of the above-mentioned reluctances have been given in [29], [33]. For simplification, the generalized MEC model shown in Fig. 5(a) can be simplified as Fig. 5(b). Φ_{st} originates from the stator windings and its leakage path consists of part of the stator tooth, the stator slot and the air-gap, thus it depends on both the MMF source and the permanent magnet flux. Assuming that the air-gap flux (Φ_g) per pole is known and remains constant, the stray magnetic flux is only dependent on the MMF source. Thus, Φ_{st} changes with the MMF sources due to the inter-turn short-circuit fault occurrence.

In order to detect and locate the inter-turn short-circuit faults inside the stator windings, the stray magnetic-flux-density (B_{st}) distribution can be measured by N TMR sensors, which are uniformly distributed outside the PMSM stator yoke. Define the magnetic flux density ratio k_n as:

$$k_n = B_{M,n} / B_{H,n} \quad (10)$$

where $B_{H,n}$ and $B_{M,n}$ denote the stray magnetic flux densities (in RMS value) of the healthy PMSM and the test PMSM possibly with inter-turn short-circuit fault, respectively, and n denotes the serial number of N sensors, which corresponds

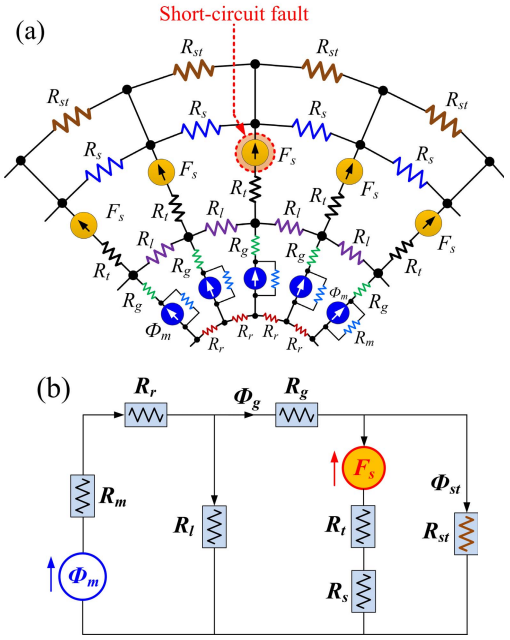

Fig. 5. (a) Generalized MEC model for SPMSM and (b) its simplified model.

TABLE I
SPECIFICATIONS OF SPMSM MODEL

Parameters	Value	Unit
Pole/slot	8/36	--
Rated phase current	8.1	A
Rated speed	1500	rpm
Rotor inertia	4.7×10^{-3}	kg·m^2
Back EMF constant	170	V/1000rpm
Winding coil resistance	0.65	Ω
Winding coil inductance	5.86	mH
Number of turns per coil	65	--

to the location of each sensor. When all of the measured k_n are equal to 1, the stator windings operate under the normal operation condition; otherwise, the windings suffer from the faulty operation with short-circuit faults. Therefore, by finding the abnormal pattern of the measured ratio k_n, the inter-turn short-circuit faults can be detected and located.

IV. FEM ANALYSIS

To validate the analytical stray magnetic field model for the inter-turn short-circuit fault detection, an SPMSM model with 8-pole/36-slot was chosen as the test motor in the simulation, as shown in Fig. 6. In order to accurately obtain the stray magnetic field distribution, totally 24 magnetic-field-sensing points (i.e., S1∼S24) were set in the simulation, which corresponded to 24 TMR sensor units uniformly distributed outside the stator yoke for sensing both radial and tangential components of stray magnetic field. The specifications of the test motor are shown in Table I. The FEM model of the test motor was simulated by the commercial software JMAG Designer 14.

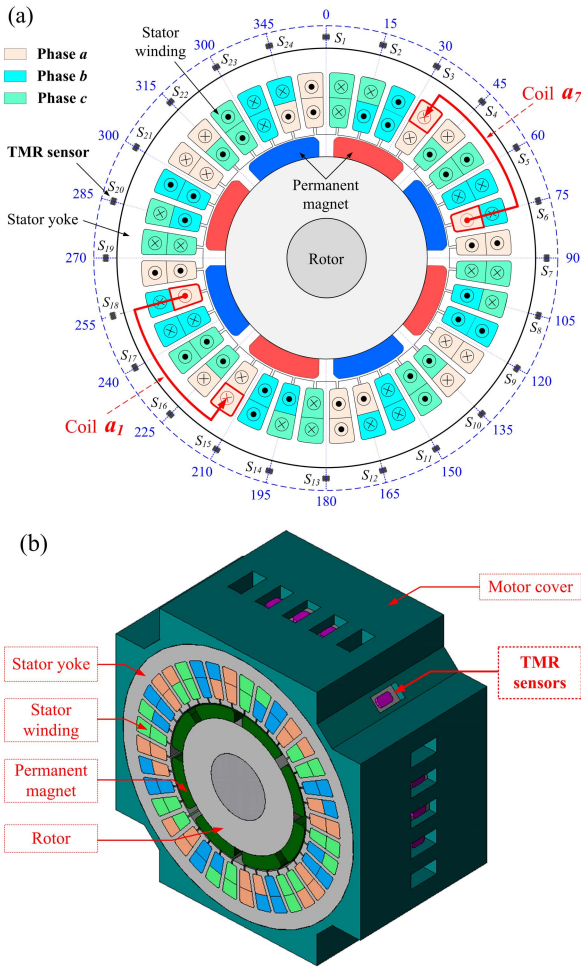

Fig. 6. SPMSM model in simulations: (a) Cross-section view. (b) 3D view.

The test motor with parallel-connected distributed windings was fed by the three-phase voltage source in the simulation, as shown in Fig. 7. Two winding short-circuit faults at different locations were alternatively set by controlling the switches S_1 and S_2. When the switch S_1 is turned on, the winding a_1 is shorted by a fault resistor R_f. Similarly, when the switch S_2 is turned on, the winding a_7 is shorted by the fault resistor R_f. The winding a_1 and a_7 are located at two different places with a 180-degree difference, as illustrated in Fig. 6(a). The resistance of the fault resistor R_f in the simulation is 0.02 Ω.

Fig. 8 shows the simulated flux vector distribution of the test motor which rotated at 1500 rpm. It can be observed that the stray magnetic flux Φ_{st} originated from the windings in stator slots and leaks outside the stator yoke. Hence, the changes in the phase currents and winding healthy conditions led to the change of Φ_{st}. Fig. 9 shows the simulation results of winding currents (i.e., i_{a1}, i_{a2} and i_{a3}), fault resistor current (i_{Rf}), radial components (B_{rad}) and tangential components (B_{tan}) of stray magnetic field at the four sensing points (i.e., S1, S7, S13 and S19). Since the windings a_1, a_2 and a_3 are series-connected in the same branch, i_{a1}, i_{a2} and i_{a3} are initially the same. A large i_{Rf} with sine waveform was rapidly induced with the same frequency of 10 Hz as the winding currents when the winding a_1 was shorted by the fault

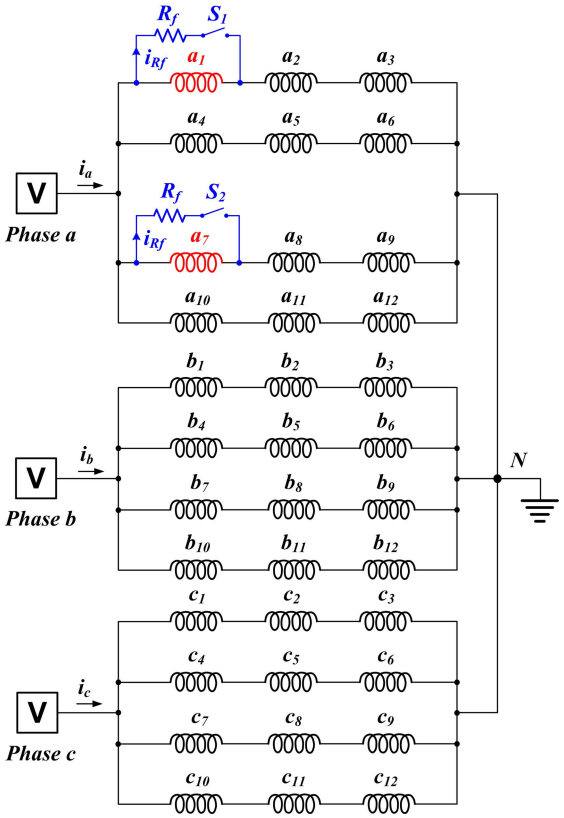

Fig. 7. Circuit model of parallel–connected windings of the test PMSM.

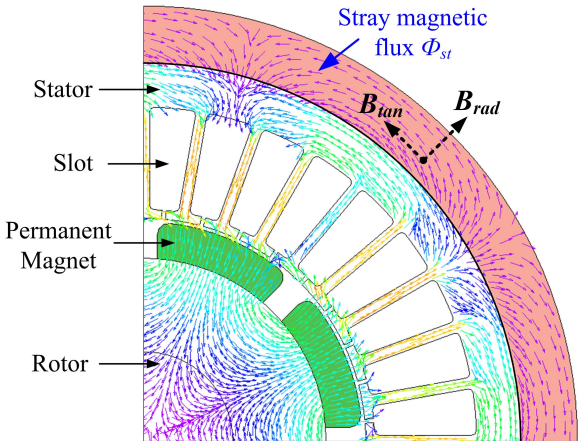

Fig. 8. Flux vector distribution showing the existence of stray magnetic flux (cross-sectional view).

resistor R_f. Meanwhile, i_{a1} rapidly dropped with the winding a_1 shorted; whereas i_{a2} and i_{a3} increased and also remained same. On the other hand, the four sensing positions S1, S7, S13 and S19 are 90-degree different so that B_{rad} and B_{tan} at these four positions are of the same phase, respectively. It can be easily found that B_{rad} and B_{tan} also changed corresponding to the occurrence of short-circuit fault. Thus, it is feasible to detect the inter-turn short-circuit fault in stator windings by sensing the stray magnetic field.

V. Experimental Verification

A. Testing Platform and TMR Sensing Technology

To experimentally verify the effectiveness of the proposed short-circuit fault detection approach, a 3.3-kW 8-pole/36-slot

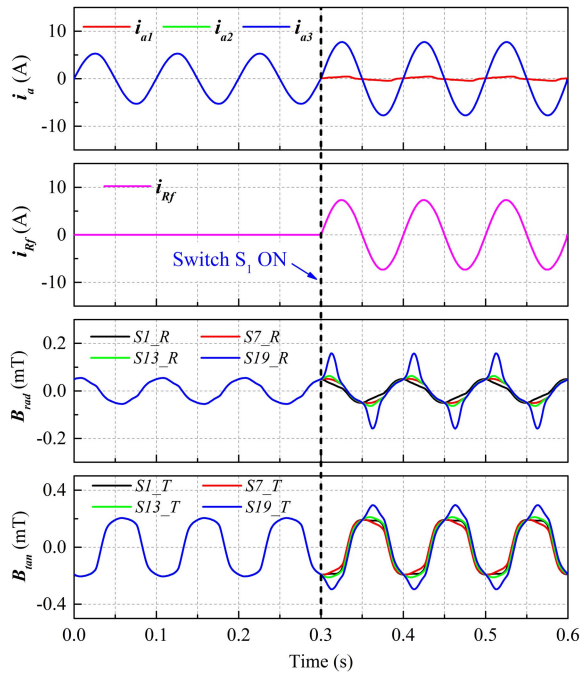

Fig. 9. Simulation results of i_a, i_{Rf}, B_{Rad} and B_{Tan} with the winding a_1 shorted.

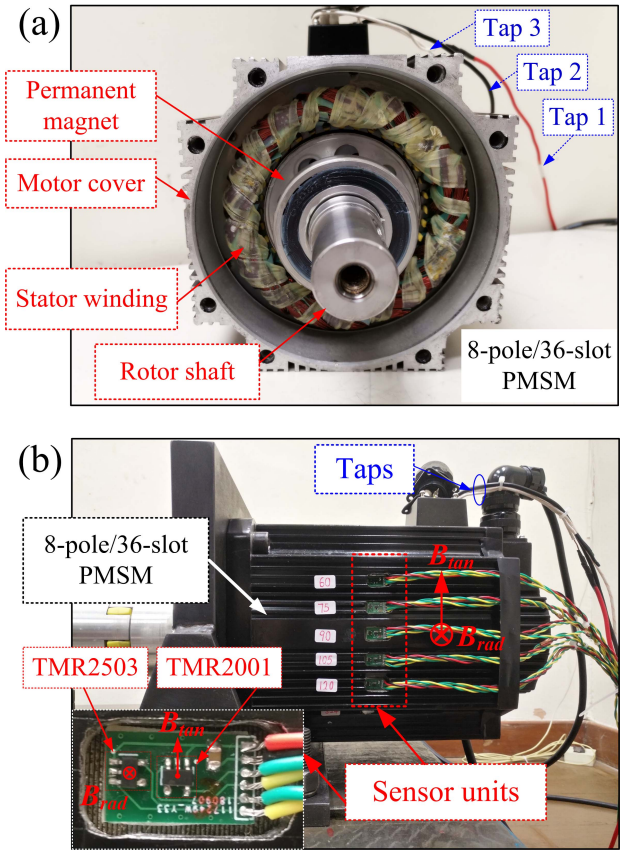

Fig. 10. (a) Test PMSM in experiments. (b) Photograph of TMR sensors mounted outside the motor stator yoke.

SPMSM was installed on the testing platform as the test motor (see Fig. 10(a)). Its main specifications and parameters are given in Table I. The SPMSM was fed through space vector

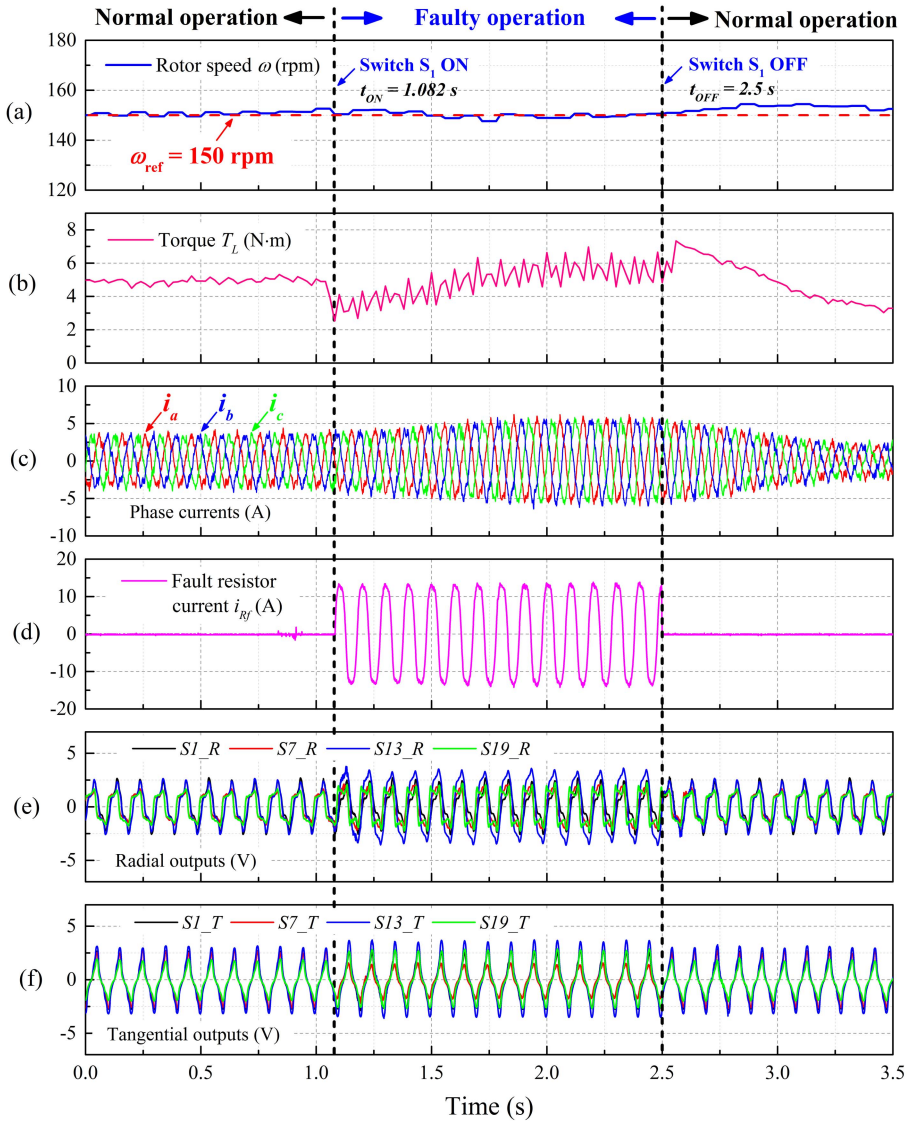

Fig. 11. Measured results under transient test with the winding a_1 shorted by a fault resistor of 0.022 Ω: (a) rotation speed ω, (b) load torque T_L, (c) phase currents (i_a, i_b and i_c), (d) fault resistor current i_{Rf}, (e) radial outputs, and (f) tangential outputs.

control using an adjustable-speed motor drive. The motor was also coupled with a high-speed flywheel and a generator to adjust the load level in experiments. During the experiments, the phase currents (i.e., i_a, i_b and i_c) of test motor as well as the fault resistor current (i_{Rf}) were monitored by four AC current probes (Tektronix TCPA300).

The three-phase parallel-connected winding configuration of the test motor is illustrated in Fig. 6 and Fig. 7. In order to simulate the inter-turn short-circuit faults in test motor, the winding a_1 and a_7 were alternatively shorted by the fault resistor R_f in experiments by controlling the switches S_1 and S_2, same as in simulation. Three electrical taps were extracted outside the motor cover to connect the switches and as fault resistors for producing the short-circuit faults (see Fig. 10(a) and Fig. 10(b)). The aluminum housed resistors (from Arcol HS series [34]) with maximum tolerance of ±10% were chosen as the fault resistors in the experiments. The resistance values of the fault resistors were also measured by a Keithley 2450 SourceMeter before the experiments. By directly using or series-connecting the fixed-value resistors, the resistances of the fault resistors in the experiments were in the range from 0.022 to 1.003 Ω.

The motor cover was drilled in order to mount 24 TMR sensor units close to the stator yoke surface for measuring the stray magnetic field, as shown in Fig. 10(b). The size of holes (i.e., 10 × 20 mm) can be possibly further reduced due to the compact size of TMR sensors (i.e., 3 × 3 × 1.45 mm SOT package). The distance between the TMR sensors and stator yoke surface is approximately 2 mm. It should be noted that the installation of TMR sensors can be completed during the fabrication stage of a new PMSM.

Two TMR sensors (i.e., TMR2001 [35] and TMR2503 [36] from Multi-Dimension Technology) were mounted on a PCB for constituting a sensor unit to measure the stray magnetic field outside the motor stator. The detailed parameters of two TMR sensors and the signal amplification gain are listed

TABLE II
SPECIFICATIONS OF TMR SENSORS IN EXPERIMENTS

Parameters	TMR2001	TMR2503	Unit
Sensitive direction	horizontal	vertical	--
Field sensitivity	80	10	mV/V/mT
Saturation field	−2.5 & 4	−70 & 70	mT
Non-linearity	1.2	0.5	%FS
Hysteresis	0.04	≤ 0.1	mT
Offset voltage	−10 ~ 10	−20 ~ 20	mV/V
Operating temperature	−40 ~ 125	−50 ~ 150	°C
Package	SOT23-5	SOT23-5	--
Amplification gain	10	50	--

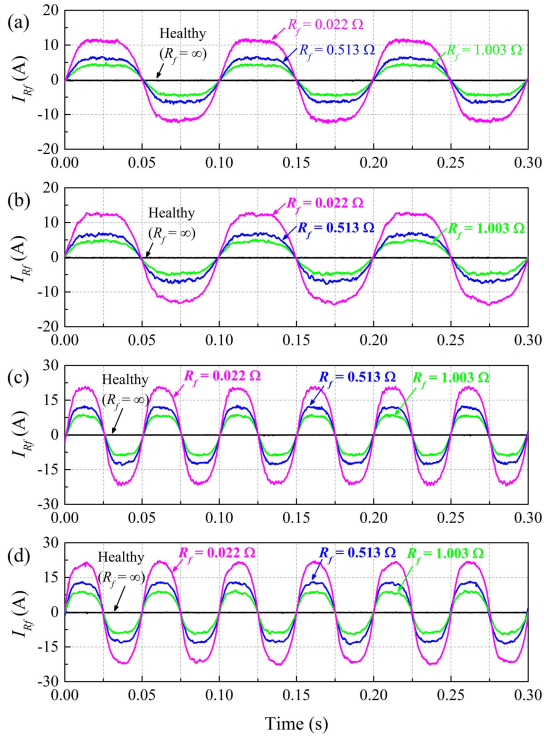

Fig. 12. Measured I_{Rf} with short-circuit faults in winding a_1: (a) $\omega = 150$ rpm, without load, (b) $\omega = 150$ rpm, $T_L = 5$ N·m, (c) $\omega = 300$ rpm, without load, (d) $\omega = 300$ rpm, $T_L = 5$ N·m.

in Table II. Each TMR sensor utilizes a push-pull Wheatstone bridge composed of four unique TMR elements. The typical magnetic-field-sensitivities of TMR2001 sensor and TMR2503 sensor are 80 mV/V/mT and 10 mV/V/mT, respectively. Moreover, the sensitive direction of TMR2001 sensor is horizontal to the sensor package, whereas that of TMR2503 sensor is perpendicular to the surface of sensor package. As the enlarged figure in Fig. 10(b) shows, the PCB with two sensors is arranged in parallel to the surface of motor stator yoke. Hence, the TMR2001 sensor and TMR2503 sensor were used to measure the tangential (B_{tan}) and radial (B_{rad}) components of the stray magnetic field, respectively. The voltage outputs of TMR sensors were amplified by the differential instrumentation amplifiers (AD620) and then filtered by a

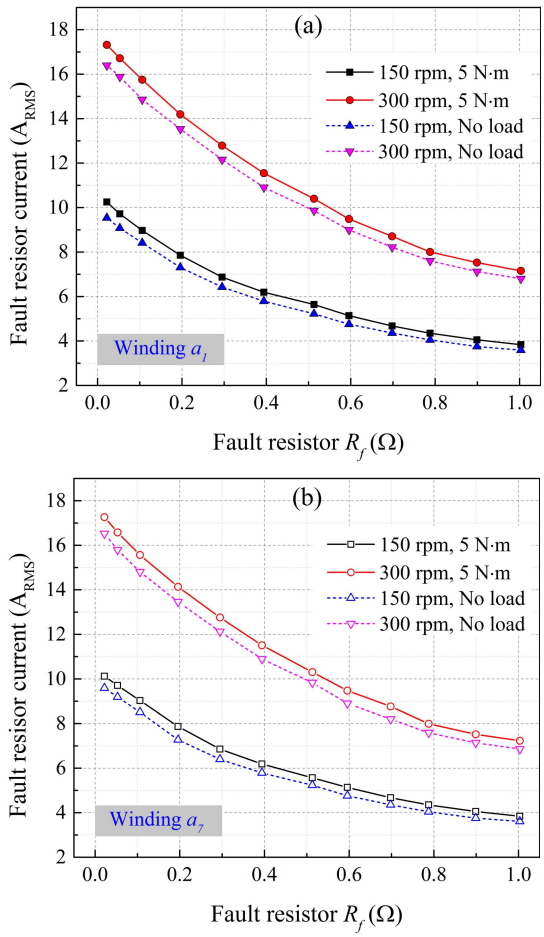

Fig. 13. Measured I_{Rf} versus R_f (a) winding a_1 Shorted and (b) winding a_7 shorted.

low-passer filter in order to eliminate the noise interface from the motor drive. The output signals were finally recorded by the 16-bit Data Acquisition unit (National Instrument NI-6225) with the sampling rate of 2 kS/s.

B. Experimental Results and Discussion

The transient test was performed to verify the proposed inter-turn short-circuit detection approach. During the transient test, the test motor with the constant rotation speed of 150 rpm encountered a short-circuit fault in the winding a_1, which was shorted by a fault resistor R_f of 0.022 Ω. The measured results under transient test are shown in Fig. 11. The test motor initially rotated at 150 rpm with load torque (T_L) of approximately 5 N·m; the stator windings operated under the normal condition, with the phase currents balanced at approximately 2.69 A_{RMS} and the fault resistor current (i_{Rf}) equaled to zero; the TMR sensors generated the uniform outputs with frequency of 10 Hz, which corresponded to the radial and tangential components of the stray magnetic field (see Fig. 11(e) and Fig. 11(f)). Here, only the outputs of the four TMR units (i.e., S1, S7, S13 and S19) among 24 sensors are demonstrated in Fig. 11. When the switch S_1 was turned on at $t = 1.082$ s, the winding a_1 is shorted by the fault resistor and the winding turned to the faulty operation.

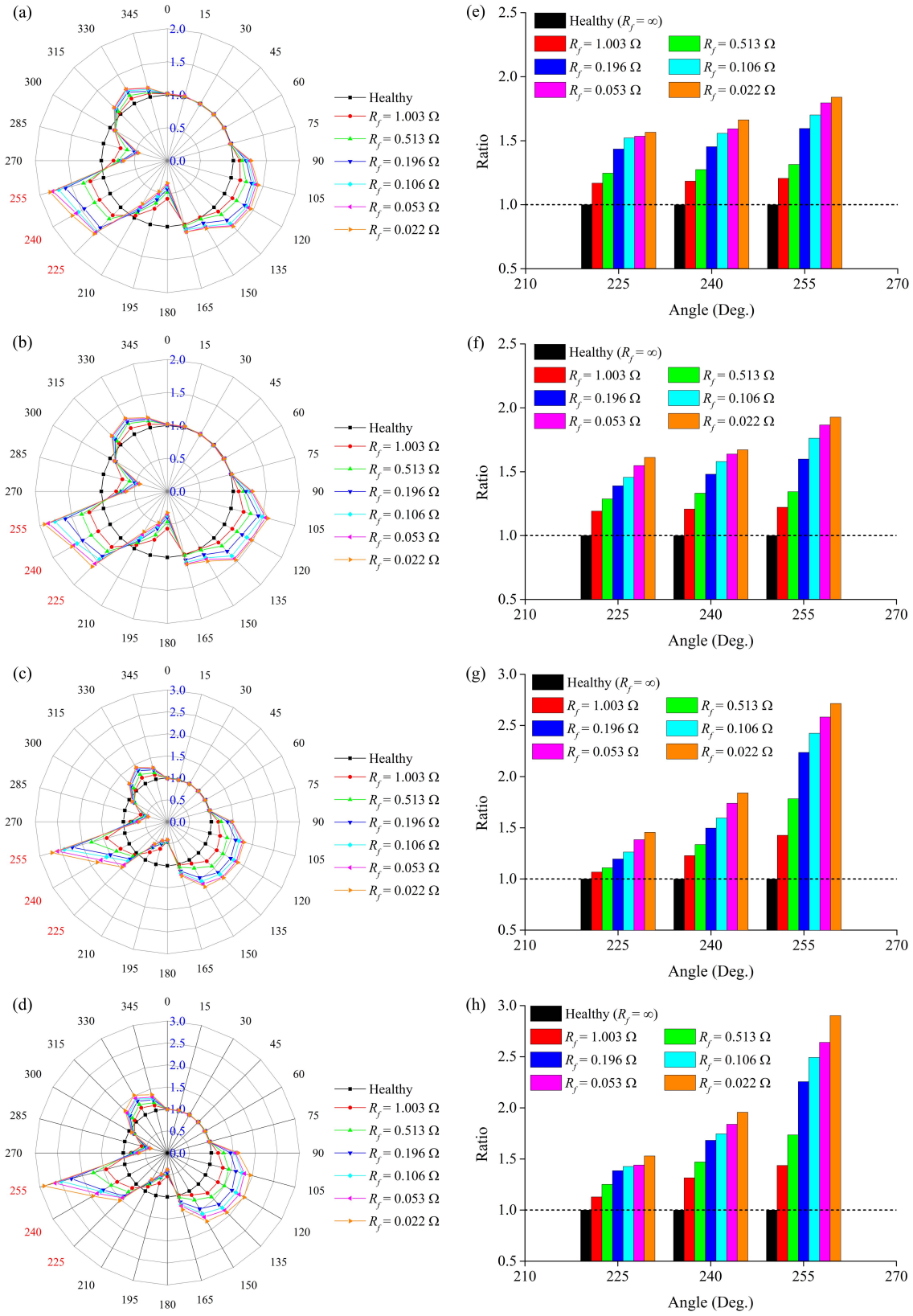

Fig. 14. Measured results of k_n with the winding a_1 shorted: (a) (e) $\omega = 150$ rpm, without load, (b) (f) $\omega = 150$ rpm, $T_L = 5$ N·m, (c) (g) $\omega = 300$ rpm, without load, and (d) (h) $\omega = 300$ rpm, $T_L = 5$ N·m.

While the test motor rotated at approximately 150 rpm, the load torque suddenly dropped to around 3 N·m and then increased gradually with large torque ripple. The phase currents also gradually increased and a large fault resistor current (i_{Rf}) of 10.3 A_{RMS} was induced with the same frequency as the phase currents (i.e., 10 Hz). On the other

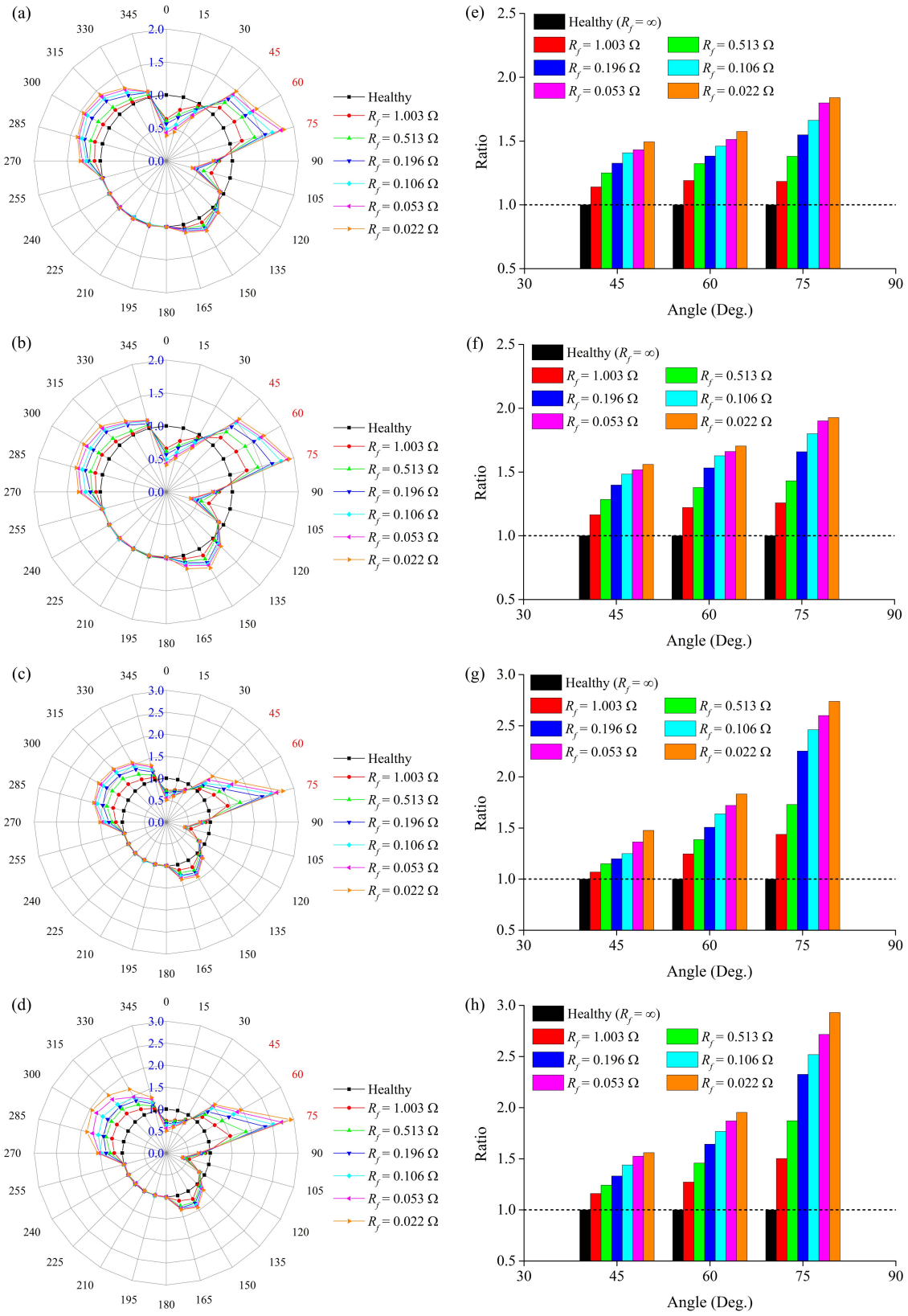

Fig. 15. Measured results of k_n with the winding a_7 shorted: (a) (e) $\omega = 150$ rpm, without load, (b) (f) $\omega = 150$ rpm, $T_L = 5$ N·m, (c) (g) $\omega = 300$ rpm, without load, and (d) (h) $\omega = 300$ rpm, $T_L = 5$ N·m.

hand, the outputs of the sensor units such as S7, S13 and S19 also suffered from the sudden changes corresponding to the short-circuit fault, which matched with the simulation results; whilst the outputs of sensor unit S1 almost remained unchanged. When the switch S_1 was turned off at $t = 2.5$ s, the stator winding a_1 recovered to the normal condition,

and i_{Rf} and sensor outputs remained the same as the initial condition. Thus, it was verified that the stray magnetic field was sensitive to the phase current change due to the inter-turn short-circuit fault. Hence, by sensing the stray magnetic field with high-sensitive TMR sensors, the inter-turn short-circuit fault can be rapidly detected.

By connecting different fault resistors (R_f) to the windings a_1 and a_7, the fault resistor currents (i_{Rf}) under short-circuit faults with different severity were also investigated. The value of i_{Rf} in this work were used to represent the severity level of short-circuit fault. Fig. 12 shows the measured results of i_{Rf} when the winding a_1 was shorted by different fault resistors, which operated under conditions with different rotation speeds (i.e., $\omega = 150$ rpm and $\omega = 300$ rpm) and load levels (i.e., without load and with constant load $T_L = 5$ N·m). i_{Rf} did not occur for a healthy winding a_1; whereas i_{Rf} with the quasi-sine wave was induced when the winding a_1 was shorted. The frequency of i_{Rf} was the same as the phase currents, which corresponded to the rotation speed (ω) of the test PMSM. The relation of i_{Rf} with R_f, ω, and T_L was illustrated in Fig. 13. As we can see, Fig. 13(a) and Fig. 13(b) show the measured i_{Rf} in RMS value when the windings a_1 and a_7 were shorted, respectively. Although the windings a_1 and a_7 were located at two places with the 180-degree difference, they possessed the same parameters such as winding resistance, inductance and turn number, and thus the values of i_{Rf} with windings a_1 and a_7 shorted by the same fault resistors were nearly same. It can also be found that smaller R_f, higher ω, and higher T_L lead to higher i_{Rf} and thus higher severity of short-circuit faults.

The stray magnetic field distribution outside the stator yoke was measured by the 24 TMR sensor units. In this work, the radial components of the stray magnetic field were used to locate the inter-turn short-circuit fault as they were more sensitive to the short-circuit fault comparing to the tangential components [29]. Fig. 14 and Fig. 15 demonstrate the measured magnetic flux density ratios k_n (based on Eq. (10)) in the radar charts with the windings a_1 and a_7 shorted, respectively. In this work, the angle resolution is 15 degree as 24 sensor units were used to measure the stray field of 360-degree. It can be seen that not all the measured values of k_n were equal to 1 when the windings a_1 and a_7 were alternatively shorted by the fault resistors with resistances from 0.022 to 1.003 Ω. The measured k_n under four faulty conditions with shorted windings a_1 and a_7 exhibited the 180-degree difference but the similar magnitudes under all four operating conditions (see Fig. 14(a)-(d) and Fig. 15(a)-(d)). As the double layer 8-pole/36-plot winding configuration with a coil span of 4 slot pitches was applied in the test SPMSM, the shorted winding produced the abnormal stray field distribution among an angle span. As illustrated in Fig. 7, there are three series-connected in each branch so that the short-circuit of winding a_1 the changes of currents through the winding a_1 as well as the windings a_2 and a_3. Similarly, the short-circuit of winding a_7 the changes of currents through the winding a_7 as well as the windings a_8 and a_9. Thus, the stray magnetic field distribution changed corresponding to the currents changes in multiple windings when the windings a_1 and a_7 were shorted. So there existed more than one peak in the magnetic flux density ratio distribution due to the distributed winding configuration of the test SPMSM, as demonstrated in Fig. 14(a)-(d) and Fig. 15(a)-(d). Hence, A fault-localization algorithm was developed in this work to process the measured values of k_n and to accurately locate the short-circuit faults in stator windings. Its detailed description is shown in Algorithm 1. According to the analysis of k_n distribution, the short-circuit fault location was recognized by finding an angle span containing the peak (where $k_n > 1$) between two adjacent valleys (where $k_n < 1$).

Using fault-localization algorithm, although under operating conditions with different rotation speeds and load levels, the short-circuit faults in the windings a_1 and a_7 were accurately localized, respectively. The short-circuit fault in shorted winding a_1 was localized between 225 and 255 degree; whilst the fault in shorted winding a_7 was localized between 45 and 75 degree. The accuracy of fault-localization in the experiments was limited by the number of TMR sensors outside the motor yoke. It can be deduced that more sensors will provide the stray magnetic field distribution with higher spatial resolution and thus more accurate fault-localization results.

Moreover, the severity of short-circuit faults can also be estimated by the measured values of k_n. As shown in Fig. 14(e)-(h) and Fig. 15(e)-(h), smaller R_f led to higher severity of inter-turn short-circuit faults, and the measured values of k_n also increased with the severity. Hence, the fault severity can be estimated from the measured values of k_n at the fault positions.

Algorithm 1 Short-Circuit Fault Localization

1) Acquire 2000 sampling points periodically from each sensors for obtaining the values of $B_{M,n}$ (in RMS value);
2) Upload the pre-determined values of $B_{H,n}$;
3) Calculate the values of k_n:
   $k_n = {B_{M,n}}/{B_{H,n}} (n = 1, 2, \cdots, 24)$
4) Update the normal values from the array of k_n: let k_n becomes into one if $0.98 \leq k_n \leq 1.02$;
5) Find the upper boundary of fault location:
   if $k_n > 1$, $k_{n+1} < 1$ and $k_{n-3} < 1$, then let U equals to n;
6) Find the lower boundary of fault location:
   if $k_{n-1} < 1$, $k_n > 1$ and $k_{n+3} < 1$, then let L equals to n;
7) Compute the angle span containing the winding location of short-circuit faults: $15L \leq Span \leq 15U$.

As a final remark, it should be noted that the proposed approach provides a promising solution to the online inter-turn short-circuit fault detection for PMSMs. Comparing to the MCSA-based detection techniques [11], [13], [14], the proposed approach is capable of accurately localizing the short-circuit faults in stator slots. The severity of short-circuit faults can also be estimated according to the changing rate of the stray magnetic field. Moreover, the sensitive TMR sensors with compact size allow the easy installation and replacement outside the motor stator yoke, surpassing the bulky search

coils that suffer from the complicated and time-consuming installation for magnetic field sensing [25], [26], [37]. This proposed approach allows the online fault diagnostics, with the PMSMs under test remaining operating. It is also worthwhile to highlight that the detection method though stray magnetic field sensing is applicable for various PMSMs with concentrated or distributed winding configurations.

VI. Conclusion

This paper presents an approach to inter-turn short-circuit fault detection for PMSMs by sensing the stray magnetic field outside the stator yoke. Both FEM simulation and experimental results have been presented to substantiate the successful application of the proposed approach. TMR sensors have been used for measuring the stray magnetic fields, which ensure the easy installation, low cost and compactness. The short-circuit fault localizations under diverse operation conditions have been demonstrated in the experiments. Thus, this proposed approach through stray field sensing provides a new perspective on the online inter-turn short-circuit diagnostics for electric machines.

References

[1] K. T. Chau, C. C. Chan, and C. Liu, "Overview of permanent-magnet brushless drives for electric and hybrid electric vehicles," *IEEE Trans. Ind. Electron.*, vol. 55, no. 6, pp. 2246–2257, Jun. 2008.

[2] M. E. Haque, M. Negnevitsky, and K. M. Muttaqi, "A novel control strategy for a variable-speed wind turbine with a permanent-magnet synchronous generator," *IEEE Trans. Ind. Appl.*, vol. 46, no. 1, pp. 331–339, Jan./Feb. 2010.

[3] R. Krishnan, *Permanent Magnet Synchronous and Brushless DC Motor Drives*. Boca Raton, FL, USA: CRC Press, 2009.

[4] J. He, C. Somogyi, A. Strandt, and N. A. O. Demerdash, "Diagnosis of stator winding short-circuit faults in an interior permanent magnet synchronous machine," in *Proc. IEEE Energy Convers. Congr. Expo. (ECCE)*, Pittsburgh, PA, USA, Sep. 2014, pp. 3125–3130.

[5] H. Henao *et al.*, "Trends in fault diagnosis for electrical machines: A review of diagnostic techniques," *IEEE Ind. Electron. Mag.*, vol. 8, no. 2, pp. 31–42, Jun. 2014.

[6] S. Moon, H. Jeong, H. Lee, and S. W. Kim, "Detection and classification of demagnetization and interturn short faults of IPMSMs," *IEEE Trans. Ind. Electron.*, vol. 64, no. 12, pp. 9433–9441, Dec. 2017.

[7] Y. Qi, M. Zafarani, B. Akin, and S. E. Fedigan, "Analysis and detection of inter-turn short-circuit fault through extended self-commissioning," *IEEE Trans. Ind. Appl.*, vol. 53, no. 3, pp. 2730–2739, May/Jun. 2017.

[8] A. Gandhi, T. Corrigan, and L. Parsa, "Recent advances in modeling and online detection of stator interturn faults in electrical motors," *IEEE Trans. Ind. Electron.*, vol. 58, no. 5, pp. 1564–1575, May 2011.

[9] J. Geiman, "DC Step-voltage and surge testing of motors," *Maintenance Technol.*, vol. 20, no. 3, p. 32, 2007.

[10] B.-G. Gu, "Study of IPMSM interturn faults part I: Development and analysis of models with series and parallel winding connections," *IEEE Trans. Power Electron.*, vol. 31, no. 8, pp. 5931–5943, Aug. 2016.

[11] B. M. Ebrahimi and J. Faiz, "Feature extraction for short-circuit fault detection in permanent-magnet synchronous motors using stator-current monitoring," *IEEE Trans. Power Electron.*, vol. 25, no. 10, pp. 2673–2682, Oct. 2010.

[12] A. G. Espinosa, J. A. Rosero, J. Cusidó, L. Romeral, and J. A. Ortega, "Fault detection by means of Hilbert–Huang transform of the stator current in a PMSM with demagnetization," *IEEE Trans. Energy Convers.*, vol. 25, no. 2, pp. 312–318, Jun. 2010.

[13] G. M. Joksimovic and J. Penman, "The detection of inter-turn short circuits in the stator windings of operating motors," *IEEE Trans. Ind. Electron.*, vol. 47, no. 5, pp. 1078–1084, Oct. 2000.

[14] N. Leboeuf, T. Boileau, B. Nahid-Mobarakeh, N. Takorabet, F. Meibody-Tabar, and G. Clerc, "Effects of imperfect manufacturing process on electromagnetic performance and online interturn fault detection in PMSMs," *IEEE Trans. Ind. Electron.*, vol. 62, no. 6, pp. 3388–3398, Jun. 2015.

[15] J. Seshadrinath, B. Singh, and B. K. Panigrahi, "Investigation of vibration signatures for multiple fault diagnosis in variable frequency drives using complex wavelets," *IEEE Trans. Power Electron.*, vol. 29, no. 2, pp. 936–945, Feb. 2014.

[16] M. A. S. K. Khan and M. A. Rahman, "Development and implementation of a novel fault diagnostic and protection technique for IPM motor drives," *IEEE Trans. Ind. Electron.*, vol. 56, no. 1, pp. 85–92, Jan. 2009.

[17] W. Guo, B.-J. Ge, Y.-P. Gao, and M.-Z. Li, "Negative-sequence component analysis of an AP1000 nuclear turbo-generator in an internal short-circuit condition," *Electr. Power Compon. Syst.*, vol. 43, no. 6, pp. 633–643, Mar. 2015.

[18] H. Jeong, S. Moon, and S. W. Kim, "An early stage interturn fault diagnosis of PMSMs by using negative-sequence components," *IEEE Trans. Ind. Electron.*, vol. 64, no. 7, pp. 5701–5708, Jul. 2017.

[19] S. Cheng, P. Zhang, and T. G. Habetler, "An impedance identification approach to sensitive detection and location of stator turn-to-turn faults in a closed-loop multiple-motor drive," *IEEE Trans. Ind. Electron.*, vol. 58, no. 5, pp. 1545–1554, May 2011.

[20] T. Boileau, N. Leboeuf, B. Nahid-Mobarakeh, and F. Meibody-Tabar, "Stator winding inter-turn fault detection using control voltages demodulation," in *Proc. IEEE Transp. Electrific. Conf. Expo*, Dearborn, MI, USA, Jun. 2012, pp. 1–6.

[21] F. Zidat, J.-P. Lecointe, F. Morganti, J.-F. Brudny, T. Jacq, and F. Streiff, "Non invasive sensors for monitoring the efficiency of AC electrical rotating machines," *Sensors*, vol. 10, no. 8, pp. 7874–7895, 2010.

[22] T. Goktas, M. Zafarani, K. W. Lee, B. Akin, and T. Sculley, "Comprehensive analysis of magnet defect fault monitoring through leakage flux," *IEEE Trans. Magn.*, vol. 53, no. 4, Apr. 2017, Art. no. 8201010.

[23] A. Ceban, R. Pusca, and R. Romary, "Study of rotor faults in induction motors using external magnetic field analysis," *IEEE Trans. Ind. Electron.*, vol. 59, no. 5, pp. 2082–2093, May 2012.

[24] M. Barzegaran, A. Mazloomzadeh, and O. A. Mohammed, "Fault diagnosis of the asynchronous machines through magnetic signature analysis using finite-element method and neural networks," *IEEE Trans. Energy Convers.*, vol. 28, no. 4, pp. 1064–1071, Dec. 2013.

[25] Y. Da, X. Shi, and M. Krishnamurthy, "A new approach to fault diagnostics for permanent magnet synchronous machines using electromagnetic signature analysis," *IEEE Trans. Power Electron.*, vol. 28, no. 8, pp. 4104–4112, Aug. 2013.

[26] H. Henao, C. Demian, and G.-A. Capolino, "A frequency-domain detection of stator winding faults in induction machines using an external flux sensor," *IEEE Trans. Ind. Electron.*, vol. 39, no. 5, pp. 1272–1279, Sep./Oct. 2003.

[27] L. Jogschies *et al.*, "Recent developments of magnetoresistive sensors for industrial applications," *Sensors*, vol. 15, no. 11, pp. 28665–28689, 2015.

[28] C. Duret and S. Ueno, "TMR: A new frontier for magnetic sensing," *NTN Tech. Rev.*, vol. 80, pp. 64–71, Oct. 2012.

[29] X. Liu, C. Liu, and P. W. T. Pong, "Velocity measurement technique for permanent magnet synchronous motors through external stray magnetic field sensing," *IEEE Sensors J.*, vol. 18, no. 10, pp. 4013–4021, May 2018.

[30] X. Liu, C. Liu, W. Han, and P. W. T. Pong, "Design and implementation of a multi-purpose TMR sensor matrix for wireless electric vehicle charging," *IEEE Sensors J.*, vol. 19, no. 5, pp. 1683–1692, Mar. 2019.

[31] I. Jeong, B. J. Hyon, and K. Nam, "Dynamic modeling and control for SPMSMs with internal turn short fault," *IEEE Trans. Power Electron.*, vol. 28, no. 7, pp. 3495–3508, Jul. 2013.

[32] B.-G. Gu, J.-H. Choi, and I.-S. Jung, "Development and analysis of interturn short fault model of PMSMs with series and parallel winding connections," *IEEE Trans. Power Electron.*, vol. 29, no. 4, pp. 2016–2026, Apr. 2014.

[33] M.-F. Hsieh and Y.-C. Hsu, "A generalized magnetic circuit modeling approach for design of surface permanent-magnet machines," *IEEE Trans. Ind. Electron.*, vol. 59, no. 2, pp. 779–792, Feb. 2012.

[34] *ARCOL/Ohmite HS Aluminium Housed Power Resistors*. Accessed: Mar. 2019. [Online]. Available: http://www.arcolresistors.com/wp-content/uploads/2014/03/HS-Datasheet.pdf

[35] *TMR2001 TMR Linear Sensor Datasheet*. Accessed: Mar. 2019. [Online]. Available: http://www.dowaytech.com/en/1944.html

[36] *TMR2503 Z-Axis TMR Linear Sensor Datasheet*. Accessed: Mar. 2019. [Online]. Available: http://www.dowaytech.com/en/1766.html

[37] P. Neti and S. Nandi, "Stator interturn fault detection of synchronous machines using field current and rotor search-coil voltage signature analysis," *IEEE Trans. Ind. Appl.*, vol. 45, no. 3, pp. 911–920, May 2009.

Xuyang Liu (S'16) received the B.Eng. degree from the University of Electronic Science and Technology of China (UESTC), Chengdu, China, in 2015. He is currently pursuing the Ph.D. degree with the Department of Electrical and Electronic Engineering, The University of Hong Kong, Hong Kong, China.

His current research interests include nondestructive testing, advanced sensing technologies, and applications of magnetoresistive magnetic field sensors in electric vehicles and wireless power transfer.

Wenchao Miao received the B.Eng. degree in electrical and electronic engineering from the University of Nottingham, U.K. He is currently pursuing the Ph.D. degree with the Department of Electrical and Electronic Engineering, The University of Hong Kong, Hong Kong.

His current research interests include the applications of magnetic sensors in power systems, fault detection in dc systems, and the condition monitoring of photovoltaic systems.

Qi Xu received the B.Eng. degree from Dalian Maritime University, Dalian, China, in 2018. He is currently pursuing the Ph.D. degree with the Department of Electrical and Electronic Engineering, The University of Hong Kong, Hong Kong.

His research interests include non-intrusive fault detection, machine learning, and the applications of magnetic sensors in microgrids.

Libing Cao (S'17) received the B.Eng. degree in electrical and electronic engineering from Zhejiang University, Hangzhou, China, in 2016. He is currently pursuing the Ph.D. degree in electrical and electronic engineering with The University of Hong Kong, Hong Kong. He has received the Hong Kong Ph.D. Fellowship to support the Ph.D. degree in 2016.

His research interests include electric machines and drives, magnetic gears, and electric vehicle technology.

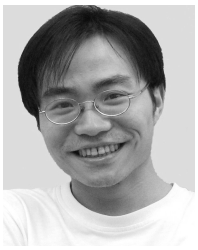

Chunhua Liu (M'10–SM'14) received the B.Eng. and M.Eng. degrees in automatic control from the Beijing Institute of Technology, China, and the Ph.D. degree in electrical and electronic engineering from The University of Hong Kong, Hong Kong, in 2002, 2005, and 2009, respectively.

He currently serves as an Assistant Professor with the School of Energy and Environment, City University of Hong Kong, Hong Kong. He has published over 180 refereed papers in his research areas. His research interests include electrical energy and power technology including electric machines and drives, electric vehicles and aircrafts, electric robotics and ships, renewable energy and microgrid, and wireless power transfer.

Dr. Liu is the Chair and Founder of HK Chapter, IEEE Vehicular Technology Society. He is currently an Associate Editor of the IEEE TRANSACTIONS ON INDUSTRIAL ELECTRONICS, an Editor of the IEEE TRANSACTIONS ON VEHICULAR TECHNOLOGY, and the Guest Editor-in-Chief of the IEEE TRANSACTIONS ON ENERGY CONVERSION. He is also an Editor of *Energies*, the Subject Editor of *IET-Renewable Power Generation*, an Associate Editor of *Cambridge University-Wireless Power Transfer*, an Associate Editor of the IEEE CHINESE JOURNAL OF ELECTRICAL ENGINEERING, and an Editor of the IEEE TRANSACTIONS ON MAGNETICS-Conference.

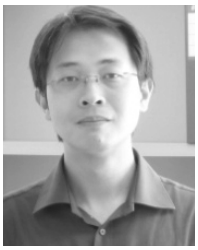

Philip W. T. Pong (SM'13) received the Ph.D. degree in engineering from the University of Cambridge in 2005.

He was a Post-Doctoral Researcher with the Magnetic Materials Group, National Institute of Standards and Technology, for three years. In 2008, he joined the Engineering Faculty, The University of Hong Kong (HKU), where he is currently an Associate Professor working on magnetoresistive sensors and their applications in smart grids and smart living. He is also a Physicist and Electrical Engineer working on magnetoresistive magnetic field sensors and smart grids with the Department of Electrical and Electronic Engineering, HKU.